

Influence of metal roughness on the near-field generated by an aperture/apertureless probe

O. J. F. MARTIN* & M. PAULUS*†

*Electromagnetic Fields and Microwave Electronics Laboratory, Swiss Federal Institute of Technology, ETH-Zentrum ETZ, CH-8092 Zurich, Switzerland

†IBM Research, Zurich Research Laboratory, CH-8803 Rüschlikon, Switzerland

Key words. Aperture probe, apertureless probe, contrast mechanisms, image formation, local probe microscopy, near-field optics, numerical simulations, scattering probe, surface roughness.

Summary

We study the influence of metal roughness on the near-field distribution generated by an aperture or an apertureless (scattering) probe. Different experimental parameters are investigated: roughness magnitude, aperture form, distribution of the roughness. Our results show that aluminium roughness has a dramatic impact on the emission characteristics of a near-field probe and in particular on its polarization sensitivity. Apertureless or scattering probes appear to be less sensitive to roughness and to provide a well confined field even with a somewhat rough probe.

Introduction

All illumination scanning near-field optical microscopy (SNOM) techniques rely on a strongly localized light source, obtained either by squeezing light through a subwavelength aperture or scattering it at a tip. In both cases, metallic surfaces, with a potential roughness, are involved.

For example, aluminium coating is generally used to define an aperture at the apex of a glass fibre. Different techniques can be used to define the tip on the bare fibre: melting–pulling (Valaskovic *et al.*, 1995), etching (Lambelet *et al.*, 1998; Stöckle *et al.*, 1999) or even bevelling (Held *et al.*, 2000). These techniques determine the overall tip shape and influence the amount of light that reaches the apex. On the other hand, the metallic aperture determines the near-field distribution and commands the resolution and contrast that can be achieved.

Tremendous efforts have therefore been made to control the aperture and the roughness of the metal that surrounds it. For example, Veerman *et al.* (1998) obtained extremely smooth

apertures in the 35–120 nm range using focused ion beam. Similar milling techniques have also been used by other groups to define or improve apertures (Muranishi *et al.*, 1997; Lacoste *et al.*, 1998).

Although it is obvious that aperture roughness has a strong impact on SNOM images, this influence is difficult to quantify. Smooth apertures have been shown to allow molecular imaging without disturbing the emission characteristics of a dipolar source (van Hulst *et al.*, 2000) or to be less polarization sensitive (Lacoste *et al.*, 1998). The objective of this paper is to address this issue from a theoretical point of view and determine the relation between the aperture roughness and the near-field distribution it generates. For completeness, we will also briefly discuss the influence of roughness for apertureless or scattering probes.

Results

The different results presented in this paper were obtained with the Green's tensor technique and we refer the reader to Martin & Piller (1998), where it is described in detail. One advantage of this approach lies in the fact that it can easily handle complex geometries, such as scatterers in a stratified background (Paulus *et al.*, 2000; Paulus & Martin, 2001). All the results were computed for a vacuum illumination wavelength of 633 nm.

Aperture probe

Let us first study the influence of a rough metallic surface on the near-field distribution generated by an aperture probe. We consider an aperture with a 100 nm nominal diameter, defined in aluminium with a 30 nm metal thickness at the aperture rim. The permittivity of aluminium at the wavelength of interest is $\epsilon = -54.2 + i19.5$ (Weaver *et al.*, 1981).

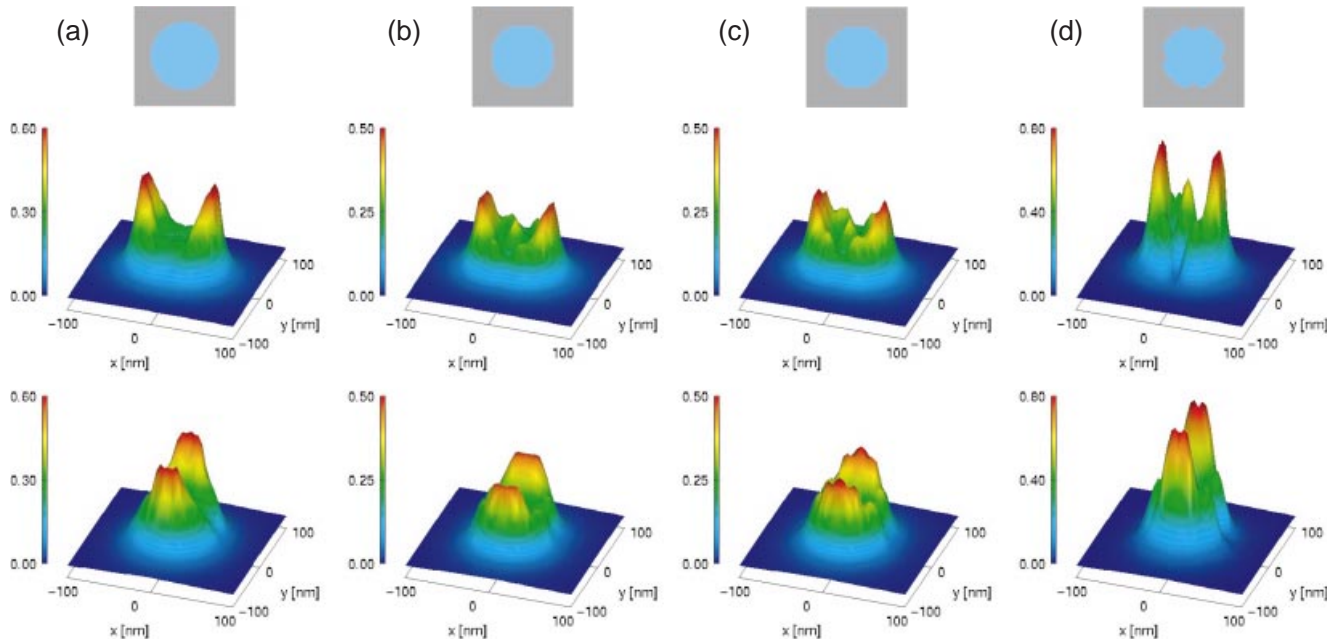


Fig. 1. Relative electric field intensity transmitted through a nominally 100 nm aperture in aluminium. The aperture is kept symmetrical and the roughness ρ increased: (a) $\rho < 2$ nm; (b) $\rho \approx 5$ nm; (c) $\rho \approx 10$ nm and (d) $\rho \approx 15$ nm. The insets show the aperture shape. Two orthogonal incident polarizations are calculated: x -polarization (top row) and y -polarization (bottom row). The same z -axis scaling is used for the intensity, i.e. the heights of the intensity distributions can be compared; by contrast, a different colourscale is used for each distribution, to cover the corresponding intensity range.

We will concentrate our attention on the influence of a rough aperture and shall not consider the effect of metallic particles deposited further away from the aperture, as such a particle primarily influences the tip motion rather than the light scattered at the aperture (Martin, 1999).

The near-field distributions are computed in a xy -plane 5 nm behind the aperture and the field intensity normalized to the illumination intensity just before the aperture. To ease comparison a similar scale is used for the z -axis (intensity axis) throughout the section (except in Fig. 3(f)) and the colour-scale is adapted to emphasize the details of each field distribution. To quantify the metal roughness ρ , we use the average roughness, as defined in Quinn (1991).

In Fig. 1 we illustrate the influence of the roughness magnitude on the near-field distribution, by increasing the roughness while keeping a very symmetrical aperture. This somewhat academic configuration helps us to understand the physical phenomena that arise in a rough aperture. For each aperture we consider separately two orthogonal linear illumination polarizations (Fig. 1).

Let us first consider the perfectly smooth aperture in Fig. 1(a) and note the two peaks in the field distribution. These peaks are located in the regions where the incident field is normal to the metallic surface (Fig. 2). They correspond to the depolarization field created during the scattering process to fulfil Maxwell's equations: the illumination electric field E in the tip being continuous, it does not fulfil Maxwell's

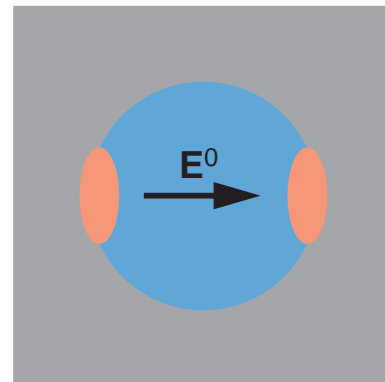


Fig. 2. To fulfil Maxwell's equations in the aperture, strong depolarization fields are generated in the regions where the incident field is normal to the core/coating interface (red areas). When the incident polarization direction is changed, these depolarization regions move (compare Fig. 1(a) top and bottom).

equations when it is normal to the core/coating interface. As a matter of fact, it is the electric displacement $D = \epsilon E$ that must be continuous in that case (Jackson, 1999). As the permittivity of the aluminium coating is much larger than that of the glass core, a strong depolarization field is created in the aperture at the core/coating interface (Fig. 2). By contrast, when the incident field is parallel to the metallic interface, it

already fulfills Maxwell's equations and no depolarization field is created (Fig. 2). If the incident polarization is rotated, the position of the peaks rotates as well (Fig. 1(a), bottom). Let us note that these depolarization fields at a material interface allow us to explain many effects observed in near-field optics (Martin *et al.*, 1996).

As long as the aperture remains symmetrical, this behaviour does not change: the two peaks associated with the depolarization follow the orientation of the incident field and the overall field distribution remains symmetrical (Figs 1(b)–(d)). However, with increasing roughness, the intensity of the depolarization peaks increases and they become narrower. We also observe a central peak that develops in the middle of the field distribution.

In an experimental configuration, the metal roughness will strongly impinge on the aperture symmetry (Lacoste *et al.*, 1998), which has a dramatic influence on the near-field distribution, as illustrated in Fig. 3. For comparison, the very smooth aperture is again reported in Fig. 3(a). A small variation in the roughness and symmetry already distorts the field significantly and additional peaks appear in the field distribution (Fig. 3(b)).

When the roughness increases, the original field distribution with two well defined peaks progressively disappears. In Figs 3(c)–(e) the field distribution occupies a large portion of the aperture rim. Furthermore, when the illumination field rotates, the field distribution no longer follows the incident polarization and some regions remain lit up independently of the illumination. For example in Fig. 3(c) only the peak visible on the left for x -polarization (top) is displaced for y -polarization (bottom), the other peaks remaining mainly unchanged.

The overall intensity transmitted through a rough aperture also strongly depends on the incident polarization: In Fig. 3(e) there is a factor of 2 between the maximum intensity for both polarizations and in the more pathological case of Fig. 3(f) there is an order of magnitude between the intensity of the x - and y -polarized fields. The importance of the depolarization fields in that last case is quite striking. A priori one could think that the field parallel to the half circle aperture can best be transmitted (Fig. 3(f) top). This is not the case and the strong depolarization fields occurring when the incident field is normal to that slit are strongly amplified and dominate the near-field (Fig. 3(f) bottom).

Such strongly disturbed and non-symmetrical field distributions will produce near-field images that are quite difficult to interpret and reflect more the topology of the aperture than that of the sample under study.

Apertureless or scattering probe

Let us now turn our attention to apertureless or scattering probes, which have proven to be a useful approach for near-field imaging (Zenhausen *et al.*, 1994; Inouye & Kawata, 1994; Bachelot *et al.*, 1995).

The metal roughness that we can expect for this type of probe is different from that relevant to aperture probes. First,

the tip is usually entirely made of metal. Second, the types of material used have a less grainy structure than aluminium. As a model we consider a tungsten tip in vacuum with an hyperboloid profile (axes $a = 10$ nm and $b = 4$ nm). This corresponds approximately to a 2 nm radius of curvature for the apex. The permittivity of tungsten at 633 nm is $\epsilon = 4.8 + i21.2$ (Weaver *et al.*, 1975). Note that only the very tip is shown in Figs 4–7; the tip used in the calculation extends further in the z -direction.

This tip is illuminated with a p -polarized incident field and the total field distribution in a xy -plane 2 nm below the apex is computed. If not otherwise specified, the incident field propagates in the y -direction.

In Fig. 4 we report the field distribution for a tip with a defect of similar material and increasing roughness. The intensity of the incident field is unity. Note the strong enhancement and confinement of the field below the tip apex. We refer the reader to Martin & Girard (1996) where this effect and its dependence on the illumination parameters have been studied in detail.

Figure 4 shows that only roughness larger than the tip apex starts to disturb the field distribution. However, even for a roughness in the order of $\rho \approx 8$ nm the radiation characteristics of the tip, with one well defined maximum, are conserved and only a small shoulder appears on the side of the field distribution (Fig. 4(f)).

The field distortions caused by the tip roughness depend of course on the location of these protrusions on the tip. However, even when the defect hangs prominently under the tip, the field distribution remains quite well confined, as illustrated in Fig. 5(a). Furthermore, as soon as the defect retracts away from the very tip, the distortions rapidly disappear. This is visible in Fig. 5(c) where the protrusion is only 2 nm above the apex.

For roughness in the order of the probe apex, the field distribution remains dictated by the lightning rod effect associated with the vertical tip extension and remains quite insensitive to the illumination direction (Fig. 6). By contrast, when the tip becomes extremely rough and irregular, the magnitude of the field can depend noticeably on the illumination direction. However, even in that case, the principal characteristics of a scattering tip are conserved and the near-field remains localized on a very small area (Fig. 7).

Conclusion

The results presented in this paper show that the tremendous efforts invested in the realization of a smooth aperture with a well defined, symmetrical shape are very worthwhile. We showed that a rough aperture has a dramatic influence on the homogeneity of the field distribution and on the polarization sensitivity of the probe, with maximum field intensity varying in extreme cases by an order of magnitude when the polarization changes by 90° .

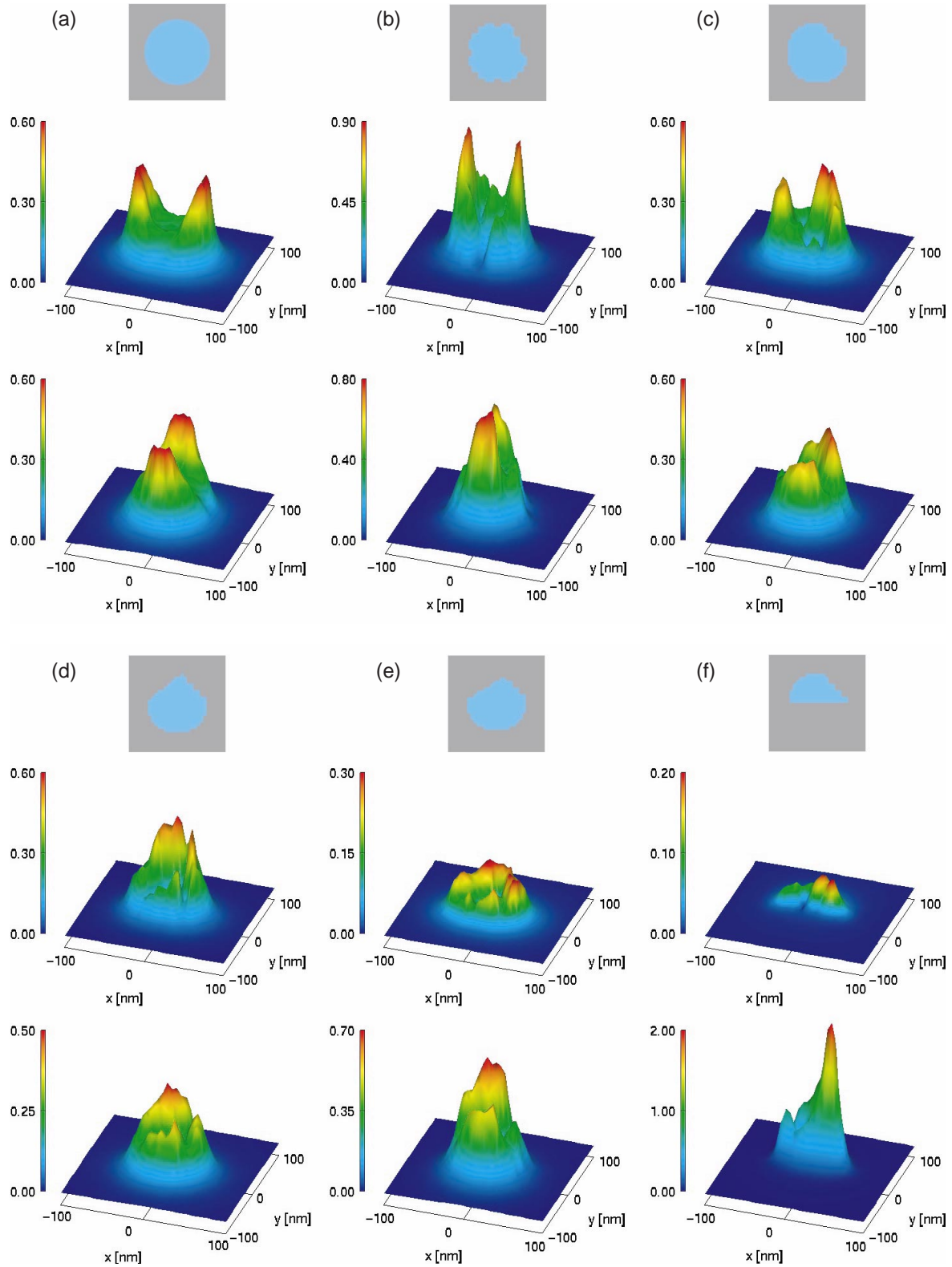


Fig. 3. Relative electric field intensity transmitted through a nominally 100 nm aperture in aluminium with different shapes (shown in the insets). The metal surface has approximately a $\rho \approx 15$ nm roughness. Two orthogonal incident polarizations are calculated: x -polarization (top row) and y -polarization (bottom row). The same z -axis scaling is used for the intensity, except in (f) where it is scaled by a factor of 0.5.

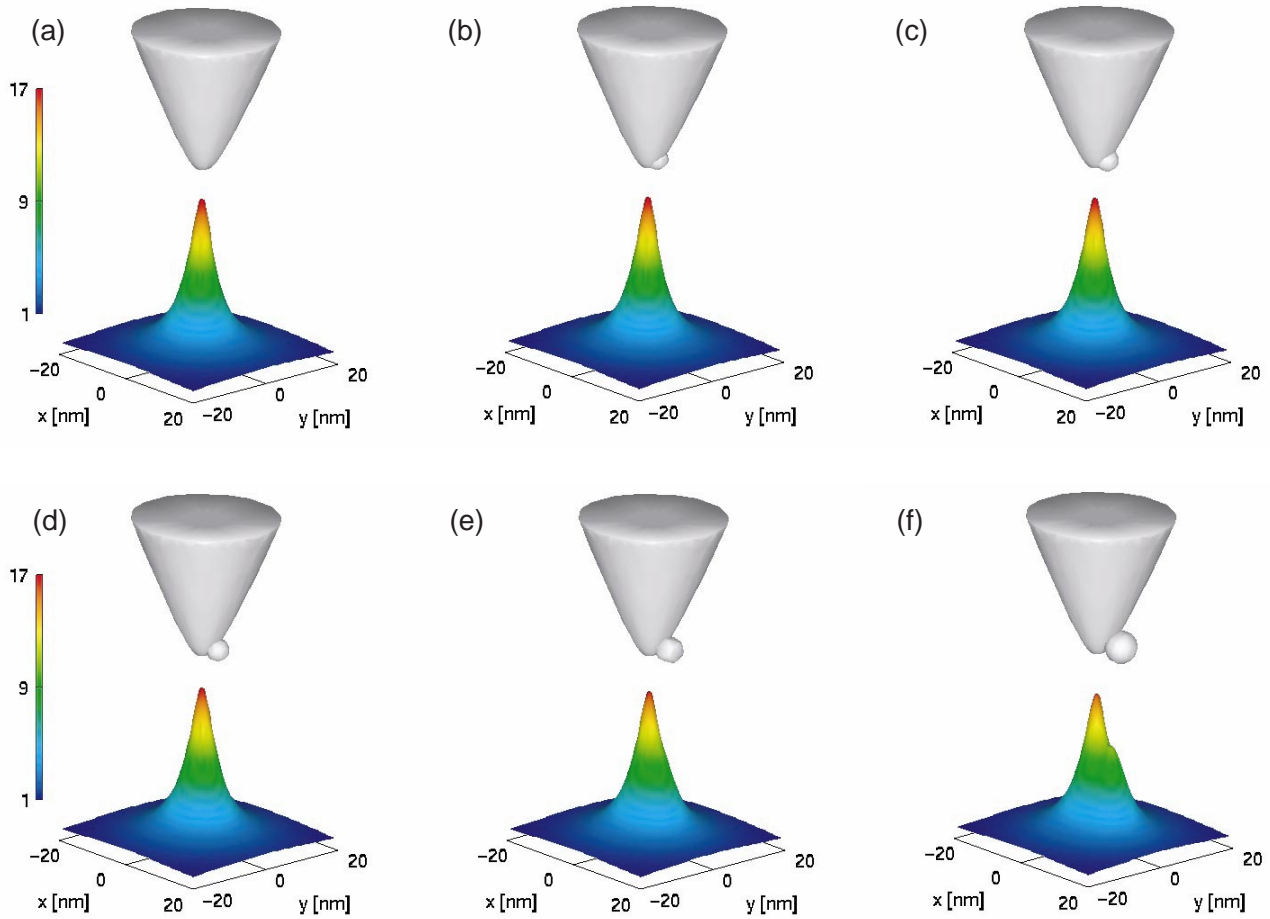


Fig. 4. Relative electric field intensity distribution 2 nm below a tungsten tip with a protrusion of similar material and increasing roughness ρ : (a) $\rho < 1$ nm; (b) $\rho \approx 2$ nm; (c) $\rho \approx 3$ nm; (d) $\rho \approx 4$ nm; (e) $\rho \approx 6$ nm; (f) $\rho \approx 8$ nm. The protrusion is located at the level of the tip apex and the system illuminated with a p-polarized wave propagating in the y -direction. The extremity of the tip is also shown.

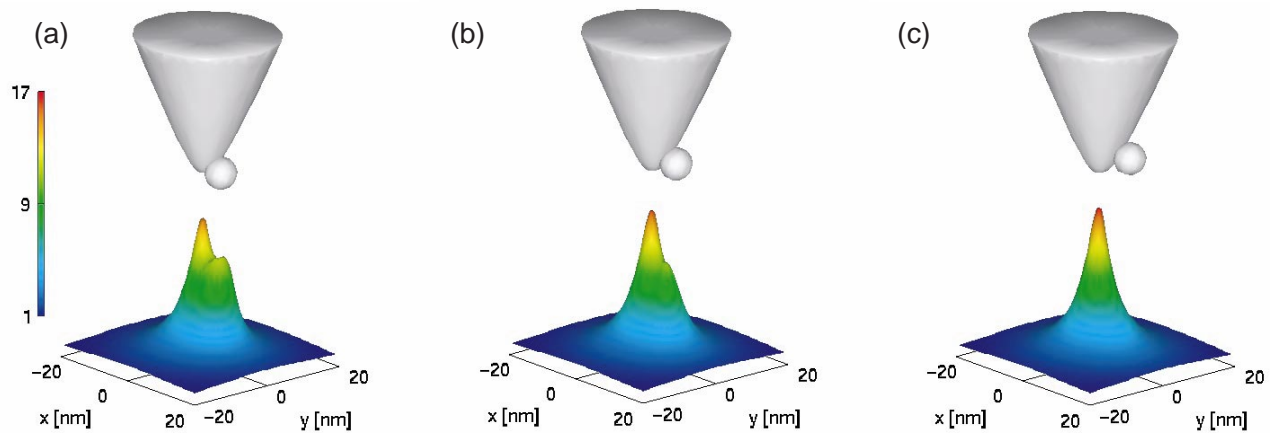


Fig. 5. Relative electric field intensity distribution 2 nm below a tungsten tip with a $\rho \approx 8$ nm protrusion located at different altitudes z relative to the apex: (a) $z = -2$ nm; (b) $z = 0$ and (c) $z = 2$ nm.

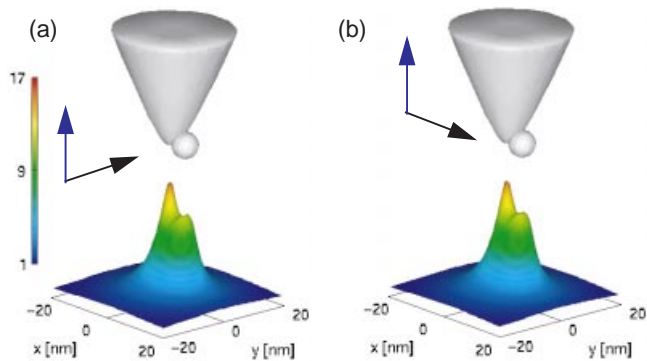


Fig. 6. Influence of the illumination direction for a tip with a $\rho \approx 8$ nm protrusion hanging 2 nm under the apex. The incident field is propagating (a) along the y -direction and (b) along the x -direction. The black arrow indicates the propagation direction of the incident field and the blue arrow its polarization.

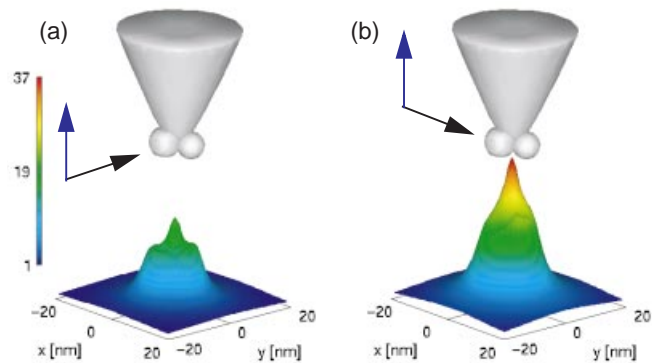


Fig. 7. Relative electric field intensity distribution 2 nm below a tungsten tip with two $\rho \approx 8$ nm protrusions hanging 2 nm under the apex. Two different illumination directions are investigated: incident field propagating (a) along the y -direction and (b) along the x -direction. The black arrow indicates the propagation direction of the incident field and the blue arrow its polarization.

This polarization sensitivity, although very disruptive for practical measurements, could be used to assess the probe roughness by simply measuring its field throughput as a function of the incident polarization.

Apertureless or scattering probes are less sensitive to surface roughness. Protrusions in the order of the very tip diameter merely disturb the scattered field, which remains confined under the apex. Only roughness located at the very tip can locally disturb the field, although even in that case the overall tip response remains determined by its vertical extension, which induces the lightning rod effect.

Acknowledgements

This work was supported by the Swiss National Science Foundation.

References

- Bachelot, R., Gleyzes, P. & Boccard, A.C. (1995) Near-field optical microscope based on local perturbation of a diffraction spot. *Opt. Lett.* **20**, 1924–1926.
- Held, T., Emonin, S., Marti, O. & Hollricher, O. (2000) Method to produce high-resolution scanning near-field optical microscope probes by beveling optical surfaces. *Rev. Sci. Instrum.* **71**, 3118–3122.
- van Hulst, N.F., Veerman, J.-A., Garcia-Parajó, M.F. & Kuipers, L.K. (2000) Analysis of individual (macro) molecules and proteins using near-field optics. *J. Chem. Phys.* **112**, 7799–7810.
- Inoué, Y. & Kawata, S. (1994) Near-field scanning optical microscope with a metallic probe tip. *Opt. Lett.* **19**, 159–161.
- Jackson, J.D. (1999) *Classical Electrodynamics*. 3rd edn. Wiley, New York.
- Lacoste, T., Huser, T., Prioll, R. & Heinzelmann, H. (1998) Contrast enhancement using polarization-modulation scanning near-field optical microscopy (PM-SNOM). *Ultramicroscopy*, **71**, 333–340.
- Lambelet, P., Savah, A., Pfeffer, A.I., Phillpona, C. & Marquis-Weible, F. (1998) Chemically etched fiber tips for near-field optical microscopy: a process for smoother tips. *Appl. Opt.* **37**, 7289–7292.
- Martin, O.J.F. (1999) 3D simulations of the experimental signal measured in near-field optical microscopy. *J. Microsc.* **194**, 235–239.
- Martin, O.J.F. & Girard, C. (1996) Controlling and tuning strong optical field gradients at a local probe microscope tip apex. *Appl. Phys. Lett.* **70**, 705–707.
- Martin, O.J.F., Girard, C. & Dereux, A. (1996) Dielectric vs. topographic contrast in near-field microscopy. *J. Opt. Soc. Am. A*, **13**, 1801–1808.
- Martin, O.J.F. & Piller, N.B. (1998) Electromagnetic scattering in polarizable backgrounds. *Phys. Rev. E*, **58**, 3909–3915.
- Muranishi, M., Sato, K., Hosaka, S., Kikukawa, A., Shintani, T. & Ito, K. (1997) Control of aperture size of optical probes for scanning near-field optical microscopy using focused ion beam technology. *Jpn. J. Appl. Phys.* **36**, L942–L944.
- Paulus, M., Gay-Balmaz, P. & Martin, O.J.F. (2000) Accurate and efficient computation of the Green's tensor for stratified media. *Phys. Rev. E*, **62**, 5797–5807.
- Paulus, M. & Martin, O.J.F. (2001) Light propagation and scattering in stratified media: a Green's tensor approach. *J. Opt. Soc. Am. A*, **18**, 854–861.
- Quinn, T.F.J. (1991) *Physical Analysts for Tribology*. Cambridge University Press, Cambridge.
- Stöckle, R., Fokas, C., Deckert, V., Zenobi, R., Sick, B., Hecht B. & Wild, U.P. (1999) High-quality near-field optical probes by tube etching. *Appl. Phys. Lett.* **75**, 160–162.
- Valaskovic, G.A., Holton, M. & Morrison, G.H. (1995) Parameter control, characterization, and optimization in the fabrication of optical fiber near-field probes. *Appl. Opt.* **34**, 1215–1228.
- Veerman, J.A., Otter, A.M., Kuipers, L. & van Hulst, N.F. (1998) High definition aperture probes for near-field optical microscopy fabricated by focused ion beam milling. *Appl. Phys. Lett.* **72**, 3115–3117.
- Weaver, J.H., Krafka, C., Lynch, D.W. & Koeh, E.E. (1981) *Optical Properties of Metal*. Physics Data, No. 18. Fachinformationzentrum Karlsruhe, Karlsruhe, Germany.
- Weaver, J.H., Olson C.G. & Lynch, D.W. (1975) Optical properties of crystalline tungsten. *Phys. Rev. B*, **12**, 1293–1297.
- Zenhausen, F., O'Boyle, M.P. & Wickramasinghe, H.K. (1994) Apertureless near-field optical microscope. *Appl. Phys. Lett.* **65**, 1623–1625.